Isotropic Events Observed with a Borehole Array in the Chelungpu Fault Zone, Taiwan

Kuo-Fong Ma *et al.*

Science **337**, 459 (2012);
DOI: 10.1126/science.1222119

Science (print ISSN 0036-8075; online ISSN 1095-9203) is published weekly, except the last week in December, by the American Association for the Advancement of Science, 1200 New York Avenue NW, Washington, DC 20005.

water ice depends on grain size, which is not an independent variable but is determined by the stress level. Unlike Europa, the tidal stress in Titan's deep interior is lower than the stress expected for convection; this means that the correct viscosity to use may be the same as that needed to transport the heat out by convection. However, the nature of the rheology at tidal frequencies is still imperfectly understood. A rocky core made weak by active dehydration and hence fracturing and the circulation of water through cracks (*9*) could also contribute to raising the value of k_2.

Alternatively, the value of k_2 contributed by the ocean itself would be enhanced if the ocean were more massive; that is, denser than the value of 1 g/cm^3 assumed for an ammonia-doped liquid water composition (*10*). A model in which the ocean has a large amount of sulfur; for example, in the form of ammonium sulfate $(NH_4)_2SO_4$; increases the ocean density by 35% (*11*), raising the value of k_2 contributed by the ocean alone to 0.57 (*2*). The value of k_2 owing to the ocean could be even higher were it not for the very thick shell required to accommodate the presence of additional ammonium sulfate (*11*).

Our results do not distinguish between the various models because of the large range of admissible values of k_2. Were one to demand that any given model provide a value of k_2 closer to the central value, a model with a low-viscosity deep interior or a sulfur-rich ocean would be required. However, these models have other problems. A low viscosity for the high-pressure ice phases of Titan's deep interior is difficult to reconcile with the values compatible with reasonable heat flows (*10*), as well as with a largely or fully differentiated rock core. The sulfur-rich ocean model (*11*) requires extensive leaching of sulfur from the core to a near-surface ocean, which is yet to be quantitatively demonstrated. A further objection to the high-density ocean model is that there is no evidence for the expected sulfur deposits on the surface (*12*). A simple water or ammonia-doped water ocean overlain by a thin (<100 km) shell is favored on various physical grounds quantified in almost all published evolution models (*13*), indirectly by the Huygens electric-field measurements (*14*), and consistent with the lowest end of the range of k_2 derived here.

References and Notes

1. L. Iess *et al.*, *Science* **327**, 1367 (2010).
2. N. Rappaport *et al.*, *Icarus* **126**, 313 (1997).
3. See the supplementary materials for additional discussion.
4. Thanks to the use of X- and Ka-band (8.4 and 32.5 GHz) frequencies and state-of-the-art instrumentation, range-rate accuracies were in the range from 2×10^{-5} to 9×10^{-5} m/s at integration times of 60 s, depending on the solar elongation angle. The dependence is due to interplanetary plasma noise, which dominates the Doppler error budget (*15*).
5. A determination of the complex Love number yields a value for Im(k_2) compatible with zero at the 1σ level. Because the flybys and their geometry were selected to maximize the sensitivity to the real part of k_2, the estimate of Im(k_2) is less stable than for the real counterpart.
6. N. Rappaport *et al.*, *Icarus* **194**, 711 (2008).
7. G. H. Darwin, *Philos. Trans. R. Soc. London* **170**, 1 (1879).
8. D. L. Goldsby, D. L. Kohlstedt, *J. Geophys. Res. Solid Earth* **106**, 11017 (2001).
9. J. C. Castillo-Rogez, J. I. Lunine, *Geophys. Res. Lett.* **37**, L20205 (2010).
10. G. Tobie, O. Grasset, J. I. Lunine, A. Mocquet, C. Sotin, *Icarus* **175**, 496 (2005).
11. A. D. Fortes, P. Grindrod, S. Trickett, L. Vocadlo, *Icarus* **188**, 139 (2007).
12. F. Paganelli *et al.*, *Planet. Space Sci.* **56**, 100 (2008).
13. F. Sohl, *Science* **327**, 1338 (2010).
14. C. Béghin, C. Sotin, M. Hamelin, *C. R. Geosci.* **342**, 425 (2010).
15. S. W. Asmar *et al.*, *Radio Sci.* **40**, RS2001 (2005).

Acknowledgments: L.I., M.D., P.R., and P.T. acknowledge support from the Italian Space Agency. The work of R.A.J., J.W.A., S.W.A., and N.J.R. was carried out at the Jet Propulsion Laboratory, California Institute of Technology, under a contract with NASA. The Doppler data used in this analysis are archived in NASA's Planetary Data System.

Supplementary Materials

www.sciencemag.org/cgi/content/full/science.1219631/DC1
Materials and Methods
Supplementary Text
Figs. S1 to S3
Tables S1 to S4
References (*16*–*20*)

25 January 2012; accepted 6 June 2012
Published online 28 June 2012;
10.1126/science.1219631

Isotropic Events Observed with a Borehole Array in the Chelungpu Fault Zone, Taiwan

Kuo-Fong Ma,[1,2]* Yen-Yu Lin,[1] Shiann-Jong Lee,[2] Jim Mori,[3] Emily E. Brodsky[4]

Shear failure is the dominant mode of earthquake-causing rock failure along faults. High fluid pressure can also potentially induce rock failure by opening cavities and cracks, but an active example of this process has not been directly observed in a fault zone. Using borehole array data collected along the low-stress Chelungpu fault zone, Taiwan, we observed several small seismic events (I-type events) in a fluid-rich permeable zone directly below the impermeable slip zone of the 1999 moment magnitude 7.6 Chi-Chi earthquake. Modeling of the events suggests an isotropic, nonshear source mechanism likely associated with natural hydraulic fractures. These seismic events may be associated with the formation of veins and other fluid features often observed in rocks surrounding fault zones and may be similar to artificially induced hydraulic fracturing.

Fluid-driven cracks and fractures are often found in the rocks surrounding fault zones and are thought to play a critical role in determining fault strength (*1*). However, the process by which these fault zone features form has not been seismically observed. Hydraulic fracturing features should be accompanied by small earthquakes with nonshearing faulting mechanisms. Analogous events have been observed seismically in volcanic and geothermal systems, as well as during artificial situations in which fluids are pumped into or out of the ground [e.g., extraction of hydrocarbons, development of enhanced geothermal energy, or storage and capture of carbon (*2*)]. The events can cluster into a pipe-like zone with dimensions up to a few hundred meters (*3*) and may be more common in low-stress environments. Because major earthquakes often result in decreased stress, recently ruptured tectonic faults provide an ideal setting to understand the active role of fluids in a low-stress environment.

In this study, we examined the Chelungpu Fault in central Taiwan (Fig. 1A), which ruptured during the 1999 moment magnitude (M_w) 7.6 Chi-Chi earthquake. We relied on data collected during The Taiwan Chelungpu-fault Drilling Project (TCDP), which produced a 2-km borehole that penetrated the fault at 1111 m (*4*), where more than 10 m of coseismic displacement (*5*) occurred. Stress measurements indicate a near zero value of shear stress on the fault after the earthquake (*6*) and are consistent with the observations from seismic and Global Positioning System modeling (*7*, *8*). We installed a seven-level array of three-component 4.5-Hz seismometers, with sampling rates of 1 kHz at the drill site across the large slip of the fault zone from depths of about 950 to 1300 m in November 2006 (Fig. 1C). The shallowest (BHS1) to deepest (BHS7) seismometers were placed at depth intervals of about 50 to 60 m. Because of the very close proximity to the fault and the low noise level in the borehole, the seismometer array allowed us to observe very-low-magnitude ($>M = -1.5$) events near the fault zone.

The continuous records (Fig. 2A) collected during the first 6 months revealed a variety of

[1]Department of Earth Sciences, and Institute of Geophysics, National Central University, Taiwan, Republic of China. [2]Institute of Earth Sciences, Academia Sinica, Taiwan, Republic of China. [3]Disaster Prevention Research Institute, Kyoto University, Japan. [4]Department of Earth Sciences, University of California Santa Cruz, Santa Cruz, CA 95060, USA.

*To whom correspondence should be addressed. E-mail: fong@ncu.edu.tw

seismic events. In addition to the regular microearthquakes, which show clear *P* and *S* waves [Fig. 2B, (*9*)], we observed several smaller events, which we call I-type (for isotropic) events, that show only distinct *P* waves without identifiable *S* waves [Fig. 2C, (*10*)]. Using a cross-correlation scheme, we found 88 detectable I-type events (cross-correlation coefficient of >0.6). The spectrum of the I-type event (Fig. 2E) has a dominant frequency of about 10 Hz. There are 30 I-type events that show distinct first motions, which can be used to locate the earthquakes (Fig. 2F). The temporal distribution of both the I-type events and the ordinary earthquakes with $t_S - t_P$ times of less than 2 s shows no time correlation (Fig. 2D).

Using the velocity structure obtained from well logs (Fig. 1C and fig. S3), we determined the locations for microearthquakes (*9*) and I-type events. These data show several low-velocity layers, including the slip zone for the 1999 Chi-Chi earthquake, within the Chinshui Shale Formation, and the layer of the Kueichulin formation (*6*, *11*–*13*). The low-velocity layer has a large Poisson ratio of about 0.34 (*14*), suggesting the possibility of fluids in these zones. We adopted a location procedure that used both the arrival times on the borehole array and the observed directions of the first motions to estimate the incidence angles (*15*). First, we used only the ordinary microearthquakes with *S* minus *P* times of less than 2 s. We located 242 events of this background seismicity, which occurred mostly in a zone at a depth of about 10 to 13 km [Fig. 1B, (*9*)], similar to the distribution of most aftershocks of the 1999 Chi-Chi earthquake (*16*). We then used the same procedure—except only *P* times were used—to locate 30 I-type events (table S1). The locations of the I-type events are mostly beneath the slip zone of the 1999 Chi-Chi earthquake (Fig. 1C) within a pipelike region that extends horizontally about 500 m northeast from the drill site (Fig. 1D), with depths from about 1300 to 1800 m. The depth range of these events corresponds to the depth of the Kueichulin Formation (Fig. 1C), which has high porosity and permeability, as constrained by laboratory measurements of the TCDP cores (*17*). From the locations and maximum amplitudes, the magnitudes of these I-type events mostly correspond to about $M = -0.5$ to $M = -1.5$ (table S1).

Several studies have shown that the anomalously low amplitudes of *S* waves in the high-frequency radiation (*18*, *19*) are associated with isotropic mechanisms; therefore, our observations of small *S* amplitude might be associated with a fault-opening motion or isotropic mechanisms in the fault zone. To further investigate the source mechanism, we carried out a three-dimensional finite-difference simulation [fig. S3, (*20*)] using six components of the moment tensors. The modeling shows that the distinct direct *S* wave is observed for each component of the moment tensor (fig. S4). The absence of an *S* wave could only be found for the case of an isotropic source, where $M_{11} = M_{22} = M_{33}$, in which only the *P* wave and other fault zone–related phases following the direct *P* wave (P_{FM}) were seen. However, there is limited azimuthal coverage of the focal sphere, so there may be some uncertainties in the source parameter determinations.

To explain the pulselike *P* wave in the observation, we used a 10-Hz oscillatory volumetric source

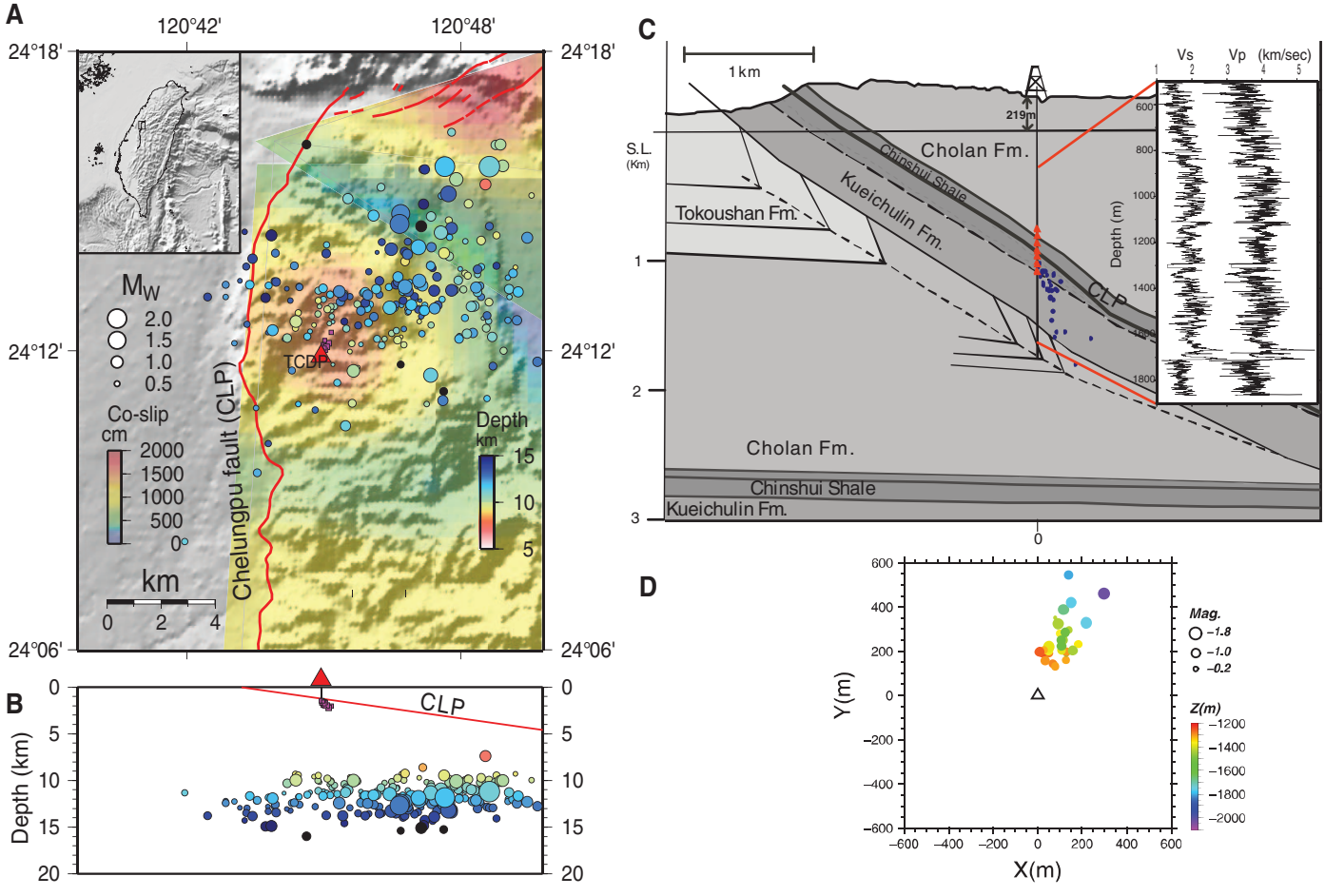

Fig. 1. (**A**) Site of the Taiwan Chelungpu-fault Drilling Project (TCDP), and borehole seismometers (BHS) on the northern portion of the Chelungpu fault (red line). The coseismic slip (color scale) is about 10 m from the drill site. The distribution of seismicity [color circles, (*9*)] and the I-type events (purple squares) are shown. (**B**) The east-west profile of the seismicity (*9*) and I-type events across the TCDP site. (**C**) A geological cross section near the drill site (*31*) with the projection of the I-type events (blue dots). The vertical borehole array (red triangles) were deployed at depths of 947, 1008, 1059, 1110, 1162, 1213, and 1274 m, respectively. The *P*-wave and *S*-wave velocities from logging are shown. (**D**) Map view of the I-type events relative to the location of the TCDP site (triangle).

in the modeling. The observed (200611201628) vertical records of BHS1 to BHS7 compares well to the seismograms calculated with the assumed velocity model (fig. S3). Using the snapshots (fig. S5) and the synthetic seismograms of the pseudo-station, we identified the arrivals in the synthetic waveforms as the direct *P*, fault zone multiples (P_{FM}), and a reflected *P*-to-*S* phase (*PS*) from the depth of 1.8 km. Although the fault zone multiples (P_{FM}) are relatively weak in the synthetic seismograms, the correlation of these multiples to the observations can be still seen (Fig. 3A). The particle motions of the direct *P* of the synthetic seismograms matches the observations, and the 1.8-km reflected phase shows a *P*-to-*S* converted phase as shown by its particle motion (Fig. 3B).

Our modeling suggests that the I-type events involved a nonshearing-type source, such as a volumetric expansion source within a 500-m distance of the TCDP drill site, and within the Kueichulin formation beneath the slip zone. Based on a nonshearing mechanism of an isotropic source of $M_{11} = M_{22} = M_{33}$, the calculated seismograms (Fig. 3C) can explain the polarities,

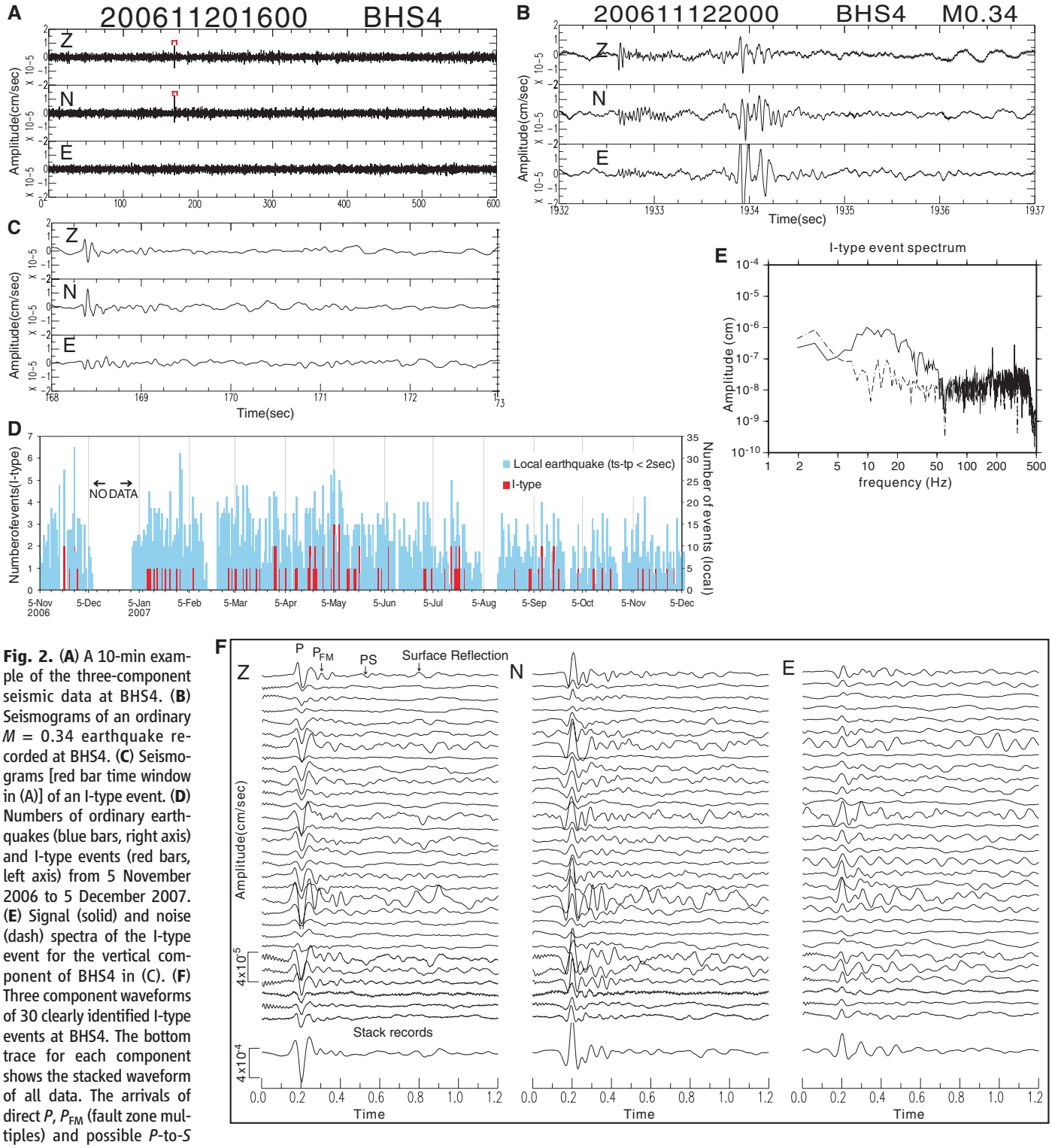

Fig. 2. (**A**) A 10-min example of the three-component seismic data at BHS4. (**B**) Seismograms of an ordinary M = 0.34 earthquake recorded at BHS4. (**C**) Seismograms [red bar time window in (A)] of an I-type event. (**D**) Numbers of ordinary earthquakes (blue bars, right axis) and I-type events (red bars, left axis) from 5 November 2006 to 5 December 2007. (**E**) Signal (solid) and noise (dash) spectra of the I-type event for the vertical component of BHS4 in (C). (**F**) Three component waveforms of 30 clearly identified I-type events at BHS4. The bottom trace for each component shows the stacked waveform of all data. The arrivals of direct *P*, P_{FM} (fault zone multiples) and possible *P*-to-*S* converted phase, and the surface reflection phase are marked.

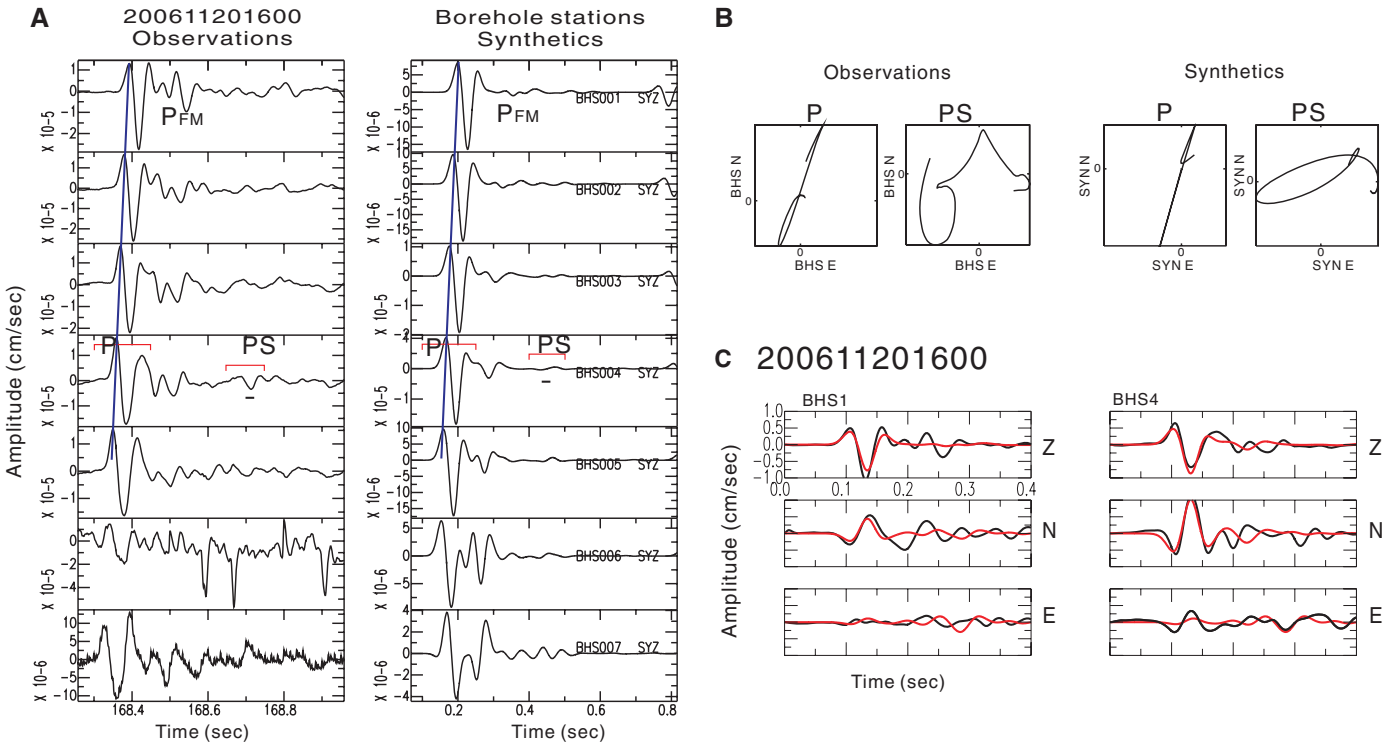

Fig. 3. (**A**) The observed (left) and calculated (right) vertical component waveforms for the seven-level borehole seismometers of the I-type event shown in Fig. 2. The bottom two borehole seismometers did not function well for the small events. The purple line shows the theoretical arrival times for the I-type event location. The possible fault zone multiples are shown with small blue and red markers. (**B**) The particle motions of the wave for *P* and *P*-to-*S* converted phase for the time windows marked by the red bars in BHS004 of (A). (**C**) Comparisons for an isotropic source of the three component waveforms of the model waveforms (red) and observations (black) at BHS1 and BHS4.

the relative amplitudes of the first arrivals in the observations, and the absence of *S* waves. We also compared a tensile failure mechanism to the observation, but the synthetics fit the observed waveforms less well than those from the isotropic mechanism (Fig. 3C and fig. S6).

Nonshearing sources are often intimately related to fluid flow. The slip zone of the 1999 earthquake itself forms an impermeable cap with permeabilities of ~10^{-19} to 10^{-16} m^2 (*21*, *22*) overlying the much more permeable Kuechulin formation with permeabilities of 10^{-14} to 10^{-13} m^2 (*17*, *23*). Despite this hydrogeological structure, fluid from the Kuechulin has been detected at the drill site (*24*). Therefore, it seems that there may be some transient flow from the capped layer, possibly related to breaching by the fracturing of the earthquake.

The occurrence of the I-type events can be explained by overpressurized fluid flow below the recent slipped zone, which is capped by the impermeable slip zone. A localized breach of the fault would provide a conduit through which fluid could escape to the overlying formations. This fluid flow results in hydraulic fractures, which result in I-type events (fig. S7). The volume change during the opening process of these events is about 30 to 300 cm^3 (*10*). This volume change corresponds to a radius of about 1 to 2.5 cm of opening and closing of cracks or cavities, which in this case, may be have been originally formed by damage during the 1999 Chi-Chi earthquake. The isotropic opening may be due to the relatively isotropic stress field remaining in the nearfield of the fault in the wake of the Chi-Chi earthquake.

Although the I-type events we observed might be a transient episode after a near-complete stress drop of a large earthquake, similar mechanisms may be appropriate for other types of fluid-driven cracks observed in the field at seismogenic depths (*25*–*27*). Furthermore, the damaged region of the fault zone (*28*) could have a strong contribution to these unusual earthquake sources. A recent study from two arrays of borehole seismometers in a carbon capture and storage experiment in the Michigan Basin also detected events with only distinct *P* waves and no *S* waves (*29*); these events had a single force mechanism associated with degassing of CO_2 due to the leakage from an injection layer. The rapid attenuation with distance of these high-frequency events (40 Hz) explains why no other I-type events at farther distances were observed by the borehole array. Indeed, fluid interaction in fracture zones could nucleate earthquakes due to stress readjustment (*30*). Regardless, if the driving mechanism of I-type events is related to fractured material and/or interaction of fluid or gas in the fault zone, such events may correspond to cross-cutting veining structures and other fluid features, such as en echelon quartz, that are often observed in rocks adjacent to fault zones.

References and Notes

1. R. H. Sibson, *Tectonophysics* **211**, 283 (1992).
2. C. T. Montgomery, M. B. Smith, *J. Pet. Technol.* **62**, 26 (2010).
3. R. J. Davies *et al.*, *Mar. Pet. Geol.* 10.1016/j.marpetgeo.2012.04.001 (2012).
4. K.-F. Ma *et al.*, *Nature* **444**, 473 (2006).
5. Y.-G. Chen *et al.*, *Bull. Seismol. Soc. Am.* **91**, 977 (2001).
6. H.-Y. Wu *et al.*, *Geophys. Res. Lett.* **34**, L01303 (2007).
7. K.-F. Ma *et al.*, *Geophys. Res. Lett.* **30**, 1244 (2003).
8. Y.-J. Hsu, P. Segall, S.-B. Yu, L.-C. Kuo, C. A. Williams, *Geophys. J. Int.* **169**, 367 (2007).
9. Y.-Y. Lin, K.-F. Ma, V. Oye, *Geophys. J. Int.* **190**, 665 (2012).
10. Materials and methods are available as supplementary materials on *Science* Online.
11. A. T. Lin *et al.*, *Terr. Atmos. Oceani. Sci.* **18**, 22 (2007).
12. E.-C. Yeh *et al.*, *Terr. Atmos. Ocean. Sci.* **18**, 327 (2007).
13. J.-H. Wang, J.-H. Hung, J. J. Dong, *J. Asian Earth Sci.* **36**, 135 (2009).
14. J.-H. Wang, *Terr. Atoms. Ocean. Sci.* **21**, 655 (2010).
15. V. Oye, M. Roth, *Comput. Geosci.* **29**, 851 (2003).
16. S. Carena, J. Suppe, H. Kao, *Geology* **30**, 935 (2002).
17. J.-J. Dong *et al.*, *Int. J. Rock Mech. Mining Sci.* **47**, 1141 (2010).
18. B. R. Julian, G. R. Foulger, *Bull. Seismol. Soc. Am.* **86**, 972 (1996).
19. A. McGarr, *Geophys. Res. Lett.* **19**, 1579 (1992).
20. S. J. Lee, H. W. Chen, K. F. Ma, *J. Geophys. Res.* **112**, B06307 (2007).
21. W. Tanikawa *et al.*, *Geochem. Geophys. Geosyst.* **10**, Q04013 (2009).
22. M. L. Doan, E. E. Brodsky, Y. Kano, K. F. Ma, *Geophys. Res. Lett.* **33**, L16317 (2006).
23. H. Tanaka *et al.*, *Terr. Atmos. Ocean. Sci.* **13**, 227 (2002).
24. C.-Y. Chen, National Taiwan University, thesis (2010).
25. R. H. Sibson, *Am. Assoc. Petrol. Geol. Mem.* **82**, 1 (2004).
26. Y. C. Chan, K. Okamoto, T.-F. Yui, Y. Iizuka, H.-T. Chu, *Terra Nova* **17**, 493 (2005).

27. F. Cappa, Y. Guglielmi, J. Virieux, *Geophys. Res. Lett.* **34**, L05301 (2007).
28. Y. Ben-Zion, J.-P. Ampuero, *Geophys. J. Int.* **178**, 1351 (2009).
29. M. Bohnhoff, M. D. Zoback, *J. Geophys. Res.* **115**, B11305 (2010).
30. F. Cappa, Y. Guglielmi, P. Fénart, V. Merrien-Soukatchoff, A. Thoraval, *Int. J. Rock Mech. Min. Sci.* **42**, 287 (2005).
31. J.-H. Hung *et al.*, *Tectonophysics* **466**, 307 (2009).

Acknowledgments: We thank C. Y. Wang for operational support for the TCDP site. This study benefited from discussions with H. Kanamori, M. Campillo, and T.-R. Alex Song. The TCDP BHS data are available to the public at the Data Center of the Taiwan Earthquake Research Center (TECDC) (http://tecws.earth.sinica.edu.tw/TCDP). This project is supported by National Science Council of Taiwan, NSC 100-2119-M-008 -031, and Ministry of Education 100G901-26 at National Central University.

Supplementary Materials
www.sciencemag.org/cgi/content/full/337/6093/459/DC1
Materials and Methods
Figs. S1 to S7
Table S1

19 March 2012; accepted 5 June 2012
10.1126/science.1222119

Adenylate Cyclases of *Trypanosoma brucei* Inhibit the Innate Immune Response of the Host

Didier Salmon,[1,2]*† Gilles Vanwalleghem,[1]† Yannick Morias,[3,4] Julie Denoeud,[5] Carsten Krumbholz,[6] Frédéric Lhommé,[7] Sabine Bachmaier,[6] Markus Kador,[6] Jasmin Gossmann,[6] Fernando Braga Stehling Dias,[1,2] Géraldine De Muylder,[1] Pierrick Uzureau,[1] Stefan Magez,[4,8] Muriel Moser,[5] Patrick De Baetselier,[3,4] Jan Van Den Abbeele,[9] Alain Beschin,[3,4] Michael Boshart,[6]* Etienne Pays[1,10]*

The parasite *Trypanosoma brucei* possesses a large family of transmembrane receptor–like adenylate cyclases. Activation of these enzymes requires the dimerization of the catalytic domain and typically occurs under stress. Using a dominant-negative strategy, we found that reducing adenylate cyclase activity by about 50% allowed trypanosome growth but reduced the parasite's ability to control the early innate immune defense of the host. Specifically, activation of trypanosome adenylate cyclase resulting from parasite phagocytosis by liver myeloid cells inhibited the synthesis of the trypanosome-controlling cytokine tumor necrosis factor–α through activation of protein kinase A in these cells. Thus, adenylate cyclase activity of lyzed trypanosomes favors early host colonization by live parasites. The role of adenylate cyclases at the host-parasite interface could explain the expansion and polymorphism of this gene family.

The protozoan flagellate *Trypanosoma brucei* infects a wide range of mammals, including humans, where it causes sleeping sickness. Bloodstream parasites are coated with a glycosylphosphatidylinositol (GPI)–anchored antigen termed variant surface glycoprotein (VSG) (*1*). Upon cellular stress, including cell lysis, activation of a GPI-specific phospholipase C (VSG lipase) triggers release of soluble VSG (*2*). Massive VSG release at the peak of parasitaemia contributes to interferon-γ (IFN-γ)–dependent tumor necrosis factor–α (TNF-α) synthesis by macrophages and high TNF-α serum levels, but early in infection, myeloid cells recruited

[1]Laboratory of Molecular Parasitology, Institute for Molecular Biology and Medicine (IBMM), Université Libre de Bruxelles, 12, rue des Professeurs Jeener et Brachet, B6041 Gosselies, Belgium. [2]Institute of Medical Biochemistry, Centro de Ciências e da Saude, Federal University of Rio de Janeiro, Avenida General Trompowsky, Rio de Janeiro 21941-590, Brazil. [3]Myeloid Cell Immunology Laboratory, Vlaams Instituut voor Biotechnologie, Brussels, Belgium. [4]Cellular and Molecular Immunology Unit, Vrije Universiteit Brussel, Brussels, Belgium. [5]Laboratory of Immunobiology, IBMM, Université Libre de Bruxelles, Gosselies, Belgium. [6]Biocenter, Section Genetics, Ludwig-Maximilians-Universität München, Martinsried, Germany. [7]Center for Microscopy and Molecular Imaging, Gosselies, Belgium. [8]Department of Structural Biology, VIB, Brussels, Belgium. [9]Department of Biomedical Sciences, Unit of Veterinary Protozoology, Institute of Tropical Medicine Antwerp, Antwerp, Belgium. [10]Walloon Excellence in Life Sciences and Biotechnology (WELBIO), Wavre, Belgium.

*To whom correspondence should be addressed. E-mail: salmon@bioqmed.ufrj.br (D.S.); boshart@lmu.de (M.B.); epays@ulb.ac.be (E.P.)
†These authors contributed equally to this work.

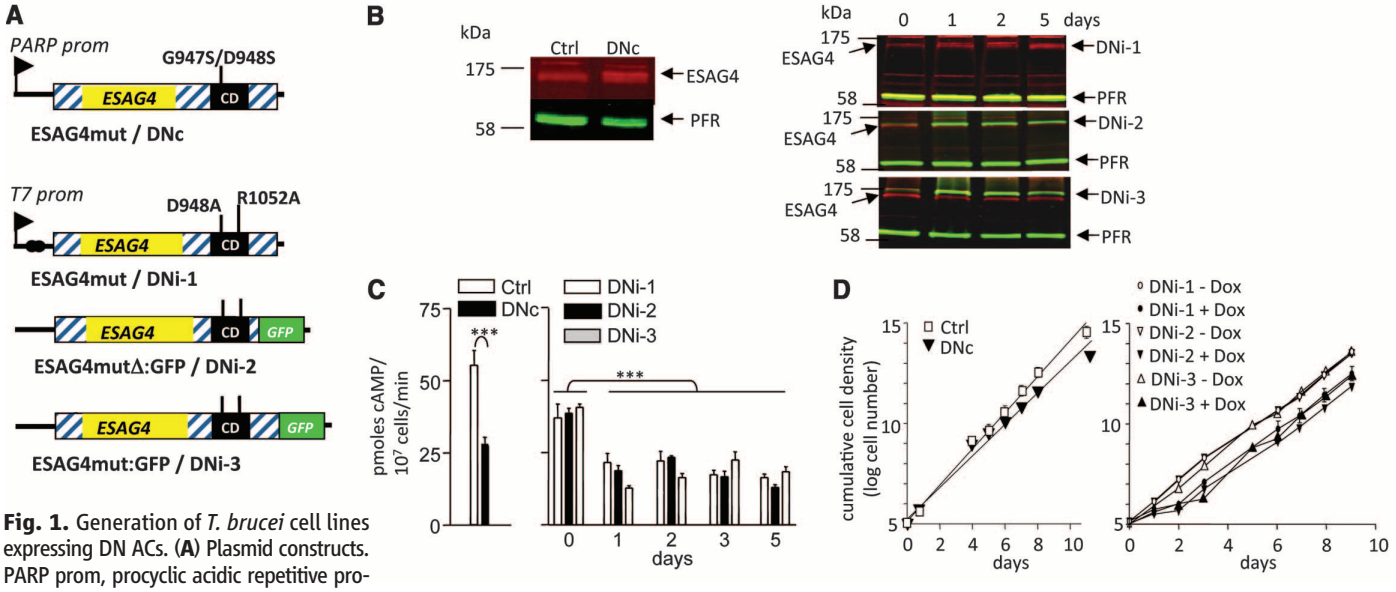

Fig. 1. Generation of *T. brucei* cell lines expressing DN ACs. (**A**) Plasmid constructs. PARP prom, procyclic acidic repetitive protein promoter; CD, catalytic domain. In DNi-2, the ESAG4 C terminus is truncated by 112 amino acids. (**B**) Immunoblot evidence for ESAG4 expression in pleomorphic DNc and monomorphic DNi parasites. Loading control: PFR, paraflagellar rod protein; d, day after doxycyclin (Dox) induction. (**C**) AC activity (cAMP synthesis), measured by swell dialysis after pH 5.5 treatment (*2*). AC activity of uninduced DNi parasites remained constant during the entire incubation period. (**D**) In vitro growth rate of the different cell lines. In this and the following figures, control (Ctrl) trypanosomes are transgenic pleomorphic trypanosomes containing an *ESAG4*-free plasmid (pTSARib0), and the values are means of at least three independent experiments (error bars, mean ± SEM). $*P < 0.05$, $**P < 0.01$, $***P < 0.001$ (Student-Newman-Keuls post hoc analysis of variance).